HHS Public Access

Author manuscript

Clin Cancer Res. Author manuscript; available in PMC 2019 October 01.

Published in final edited form as:

Clin Cancer Res. 2018 October 01; 24(19): 4900–4912. doi:10.1158/1078-0432.CCR-17-3872.

Chemotherapy sensitizes therapy-resistant cells to mild hyperthermia by suppressing heat shock protein 27 expression in triple negative breast cancer

Chaofeng Mu[#1,2], **Xiaoyan Wu**[#1,3], **Xinyu Zhou**[1], **Joy Wolfram**[1], **Jianliang Shen**[1,4], **Dechen Zhang**[1], **Junhua Mai**[1], **Xiaojun Xia**[1], **Ashley M. Holder**[1,5], **Mauro Ferrari**[1,6], **Xuewu Liu**[1], and **Haifa Shen**[1,7,8]

[1]Department of Nanomedicine, Houston Methodist Research Institute, Houston, Texas 77030, USA

[2]Department of Pharmaceutics, College of Pharmacy, Zhejiang Chinese Medical University, Hangzhou, 310053, China

[3]Department of Pediatrics, Union Hospital, Tongji Medical College, Huazhong University of Science and Technology, Wuhan, 430022, China

[4]State key laboratory of ophthalmology, School of Biomedical Engineering, Wenzhou Medical University, Wenzhou, 325035, China

[5]Department of Surgery, Houston Methodist Hospital, Houston, Texas 77030, USA

[6]Department of Medicine, Weill Cornell Medical College, New York, New York 10065, USA

[7]Department of Cell and Developmental Biology, Weill Cornell Medical College, New York, New York 10065, USA

[8]Department of Cancer Center, Houston Methodist Hospital, Houston, Texas 77030, USA

[#] These authors contributed equally to this work.

ABSTRACT

Purpose: Triple-negative breast cancer (TNBC) is a clinically aggressive disease with poor prognosis. Conventional chemotherapeutics are generally able to shrink the tumor mass, but often fail to completely eradicate cancer stem-like cells (CSCs) that are responsible for high risk of relapse and frequent metastases. In this study, we examined thermal sensibility of CSCs, developed an approach that enabled concurrent elimination of both the bulk of cancer cells and CSCs, and investigated the underlying mechanism.

Experimental Design: We designed a platform consisting of gold nanoparticle-coated porous silicon microparticle (AuPSM) that was also loaded with docetaxel micelles (mDTX) to enable concurrent killing of the bulk of cancer cells by released mDTX and CSCs by mild hyperthermia upon stimulation of AuPSM with near infrared. In addition, we examined the role of heat shock

Corresponding Author: Haifa Shen, Department of Nanomedicine, Houston Methodist Research Institute, 6670 Bertner Ave., Houston, Texas 77030. Phone: 713-441-7321; Fax: 713-441-3655; hshen@houstonmethodist.org.

Conflict of interest statement: The authors disclose no potential conflict of interest.

proteins in sensitizing CSC killing. Finally, we applied mDTX-loaded AuPSM to treat mice with SUM159 and 4T1 orthotopic tumors, and evaluated tumor growth and tumor metastasis.

Results: MDA-MB-231 and SUM159 TNBC cells treated with mDTX-loaded AuPSM and mild hyperthermia displayed significantly reduced efficiencies in mammosphere formation than those treated with mDTX alone or mild hyperthermia alone. Combination treatment also completely inhibited SUM159 orthotopic tumor growth and 4T1 tumor metastasis. Mechanistically, DTX treatment suppressed expression of heat shock protein 27 in cancer cells including the CSCs, rendering cells sensitive to mild hyperthermia.

Conclusions: Our results indicate that chemotherapy sensitizes CSC to mild hyperthermia. We have developed an effective therapeutic approach to eliminate therapy-resistant cells in TNBC.

Keywords

therapy resistance; cancer stem cell; thermal therapy; heat shock protein

INTRODUCTION

Triple negative breast cancer (TNBC) cells lack expression of estrogen receptor, progesterone receptor, and the human epidermal growth factor receptor 2. It is a heterogeneous and aggressive disease for which there is no effective targeted therapy for most cancer patients [1, 2]. Compared to hormone receptor- or human epidermal growth factor receptor 2 (HER2)-positive breast cancers, TNBC has a higher percentage of cancer stem-like cells (CSCs) [3], a subpopulation that has the ability for unlimited self-renewal and also differentiation into cells that constitute the bulk of the tumor tissue [4, 5]. CSCs are a group of cancer cells with heterogeneous surface markers and cellular functions [6–8]. They are usually not actively proliferating, and thus not sensitive to chemotherapy drugs that target the replicating cells more effectively [9–11]. In addition, CSCs can express high levels of adenosine triphosphate-binding cassette transporters that are associated with multidrug resistance [12], or activate the DNA damage response machinery to effectively reduce the impact from genome-targeting agents [13]. Such protective mechanisms ultimately reduce overall therapeutic efficacy of the cancer drugs [11, 14].

Given the essential role of CSCs on cancer growth, metastasis, and tumor recurrence, it is critical to eliminate this population of cells so as to achieve long-term disease-free survival. Several therapeutic approaches have been explored to target key signal pathways that are involved in self-renewal of CSCs [15, 16], cell metabolism [17], and cell apoptosis [18–20]. Since CSCs carry unique surface markers such as $CD44^{+}CD24^{-}$ [5], $CD133^{+}$ [21–23], and aldehyde dehydrogenase-1 (ALDH1) [24], they can also be selectively targeted, as in the case of CD44-targeted therapy [25, 26]. Chemotherapy has also been combined with targeted therapy drugs in order to enhance CSC killing activity [27]. Success in these treatment strategies requires effective drug penetration in the tumor tissue, especially in the hypoxic tumor environment with poor vasculature, so that the CSCs can receive a sufficient amount of therapeutic agents. However, the existence of multiple biological barriers, both at the systemic level and within the tumor tissue, poses a challenge for effective drug delivery [28].

Thermotherapy has been found to be a feasible approach to human cancer treatment [29]. In contrast to small molecule inhibitors and therapeutic antibody drugs, thermotherapy is not restricted by the individual signal transduction pathways that determine cancer cell viability, and thus is applicable to various cancer types with different genetic background and mutation status. To support this notion, it has been demonstrated that the TNBC CSCs are more resistant to ionizing radiation than the bulk of the tumor cells; however, these cells are equally sensitive to radiation treatment after local hyperthermia for 20 minutes at 42°C triggered by optically activated gold nanoshells [30]. One potential side effect from thermal therapy is the expression of heat shock proteins (HSPs), such as HSP27, HSP70 and HSP90 [31]. HSP27, also known as heat shock protein beta-1 (HSPB1), is a molecular chaperone that mediates cellular responses to stress conditions such as accumulation of reactive oxygen species [32]. It is constitutively activated in CSCs under hypoxia and is required to mediate resistance to apoptosis [33]. It has been reported that suppression of HSP27 can induce long-term dormancy in breast cancer [34]. Suppressing HSP expression during thermotherapy is expected to achieve an even greater therapeutic efficacy.

In this study, we observed synergistic killing of TNBC CSCs by a combination of mild hyperthermia and the chemotherapy drug docetaxel (DTX) in cell-based studies. We then developed a platform to enable concurrent drug release and mild hyperthermia inside the tumor tissue. This platform is comprised of porous silicon microparticles with gold nanoparticle deposit on surface and inside the nanopores (AuPSM). AuPSM was then loaded with DTX that was encapsulated in polymeric micelles. Once delivered to the tumor tissue, DTX micelles were released from the microparticles, and mild hyperthermia was generated by treating the AuPSM-containing tumor with near infrared laser. Anticancer effect was evaluated, and HSP27-dependent cell killing was examined.

MATERIALS AND METHODS

Reagents

Reagents were obtained from the following sources: mPEG2000-b-PLA2200 (mPEG-PLA, PI=1.09) from Polymer Source Inc. (Montreal, QC, Canada); docetaxel from LC Laboratories Inc. (Woburn, MA, US); polyvinylpyrrolidone (PVP, average MW: 58,000, K29–32) from Acros Organics (Belgium, NJ, US); auric trichloride and 3-[4,5-dimethylthiazol-2-yl]-2,5 diphenyl tetrazolium bromide (MTT) from Sigma (St. Louis, MO, US); and fetal bovine serum (FBS) from Life Technologies Inc. (Carlsbad, CA, US). All other reagents were of analytical grade from commercial sources and used without further purification.

Cell culture

MDA-MB-231 human breast cancer cells and 4T1 murine mammary gland tumor cells were purchased from the American Type Culture Collection (Rockville, MD, US). MDA-MB-231 cells were cultured in Dulbecco’s modified Eagle’s medium (DMEM) supplemented with 10% FBS. 4T1 cells were cultured in RPMI1640 medium supplemented with 10% FBS. SUM159 cells were obtained from Dr. Stephen Ethier (Kramanos Institute, MI, US). Cells were maintained in Ham’s F-12 medium with 5% FBS, 5 μg/mL insulin, and 1 μg/mL

hydrocortisone. All cell culture media were supplemented with 100 units/mL penicillin, 100 μg/mL streptomycin, and 2 mM glutamine. Cell culture was maintained in a humidified incubator with 5% CO_2 at 37°C. Each cell line was authenticated and regularly tested for mycoplasma contamination.

Cytotoxicity and ALDH1 activity assay *in vitro*

MDA-MB-231 and SUM159 cells were seeded in 96-well plates at a density of 5,000 cells per well. After an overnight incubation, cells were treated with different concentrations of docetaxel for 72 hours. Cell viability was measured using MTT assay. ALDH1 activity in MDA-MB-231 and SUM159 cells was determined with the aldefluor assay according to manufacturer's instruction (STEMCELL Technologies). Briefly, 1×10^6 cells were suspended in 1 mL of aldefluor assay buffer containing activated aldefluor substrate. Cells were centrifuged at 2,500 rpm for 5 min after incubation at 37°C for 40 min, and then resuspended in 0.4 mL aldefluor assay buffer before they were analyzed with a BD LSRII flow cytometer (BD Sciences). Cells treated with diethylaminobenzaldehyde (DEAB) in the ALDH1 staining buffer served as a control. To collect ALDH1-positive cells, cells were sorted with a BD FACSAria II Cell Sorter (BD Sciences). Apoptotic ALDH1-positive cells were detected with Annexin V staining (eBioscience) using flow cytometry.

Particle fabrication and characterization

Porous silicon microparticles (PSMs) were fabricated by a combination of electrochemical etching and photolithography as previously described [35], and processed to deposit gold nanoparticles on surface and inside the nanopores. Briefly, PSMs were dispersed in a 10% PVP solution and treated with drop-by-drop addition of an auric trichloride solution (0.1 mM) while under sonication. The suspension was left overnight at 20°C to complete gold nanoparticle formation on surface of silicon. Number of gold nanoparticle-deposited PSM (AuPSM) was determined using a Multisizer 4 Coulter Particle Counter (Beckman Coulter, USA). Morphological analysis was performed with a scanning electron microscopy (FEI NovaNanoSEM 230).

Preparation of drug-encapsulated polymeric micelles and assembly into AuPSM

A co-solvent evaporation method was applied to prepare DTX-encapsulated mPEG-PLA micelles as previously described [36]. Briefly, mPEG-PLA and DTX (6%, w/w) were dissolved in acetone, and added drop-by-drop to distilled water. After the suspension was stirred for 2 hours, acetone was removed in a vacuum chamber and the micellar solution was filtered through a 0.45 μm syringe filter to remove free drug molecules. Size and zeta potential of the micelles were determined using a Malvern Zetasizer Nano-ZS (Malvern Instruments Ltd., Worcestershire, UK). DTX content inside the micelles was measured with high-performance liquid chromatography (HPLC) using a LaChrom Elite HPLC System (Hitachi, Japan) with a C18 column (250 × 4.6 mm, 5μm, Agilent) using an acetonitrile: water mixture (55:45, v/v) as the solvent at a flow rate of 1.0 mL/min. To load micelles into AuPSM, micelles were mixed with AuPSMs and sonicated for 3 min. Coumarin-6 labeled micelles were loaded into AuPSMs and loading efficiency was measured based on fluorescent intensity with a Multi-Mode Microplate Reader (BioTek, VT). To determine

docetaxel content in AuPSM, the drug-loaded AuPSM particles were dissolved in phosphate saline buffer (pH 8.5), and concentration of released docetaxel was measured with HPLC.

Photothermal effects in aqueous suspension

Optical properties of both empty AuPSMs and AuPSMs loaded with micelles were measured using a DU® 730 UV/VIS spectrophotometer (Beckman Coulter Inc, CA). Optical absorption spectra were recorded within 400–1000 nm wavelength range. To evaluate photothermal capacity, a 300 μL AuPSM/mDTX suspension (0.15 billion particles/mL) was placed into a microtube and treated with near infrared (NIR) laser beam at a wavelength of 810 nm generated with a Delta-30 laser (AngioDynamics Inc, NY). A thermocouple was inserted into the solution to record temperature changes within a 10 min period.

Cytotoxicity *in vitro*

MDA-MB-231 and SUM159 cells were seeded in 96-well plates at a density of 5,000 cells/well. After an overnight incubation, cells were treated with AuPSM or AuPSM/mDTX for 72 hours. They were then irradiated with NIR light at an output power of 2 W for 3 min. Cell viability was measured using MTT assay 24 hours after irradiation. Cells were also seeded in 4-well chamber slides (Lab-Tek II, Nunc) at a density of 2×10^4 cells/well and exposed to the same treatment as described above. Live and dead cells were then stained with calcein acetoxymethyl ester and ethidium homodimer, respectively, following the manufacturer's instructions (Invitrogen). Cells were imaged using an Olympus IX81 inverted fluorescence microscope.

Mammosphere formation in cell culture

Single tumor cells were isolated from breast tumor tissues following a previously reported protocol with modifications [37]. Briefly, SUM159 or MDA-MB-231 tumors were minced and digested in 10 mL of DMEM/F12 medium containing collagenase (300 U/mL), gentamicin (100 mg/mL), and 1% antibiotic-antimycotic solution (Invitrogen) for 1.5 hours at 37°C. The resultant cell suspension was filtered through a 40-μm mesh (BD Falcon) to obtain single cells. Cells were then resuspended in serum-free STEM cell medium (STEMCELL Technologies) containing hydrocortisone (0.5 g/mL) and heparin (0.5 U/mL), and seeded into 96-well ultra-low attachment plates (Corning) at a density of 1,000 cells/well to form mammospheres. After 7 days, the primary mammospheres were digested, and single cells were resuspended in the serum-free STEM cell medium and seeded into 96-well ultra-low attachment plates at a density of 1,000 cells/well to form secondary mammospheres. To set up cell culture for drug treatment, single cells from second mammospheres were treated with particles with or without DTX followed by NIR laser treatment (2 W for 3 min) 72 hours later. The post-treatment cells were seeded in ultra-low attachment plates, and number of mammospheres per well was determined seven days later.

Heat shock protein (HSP) expression analysis

To knock down HSP27 expression, SUM159 cells were transfected with a scrambled siRNA (siScr: 5'-CAGCGCUGACAACAGUUUCAU-3') or Hsp27-specific siRNA (siHSP27: 5'-GUCUCAUCGGAUUUUGCAGC-3') [38] using Lipofectamine® RNAiMAX (Invitrogen)

for 72 hours. To overexpress HSP27, SUM159 cells were transfected with pCMV6-Entry/HSPB1 (OriGene Technologies) using Lipofectamine® 2000 (Invitrogen) for 48 to 72 hours. To measure protein levels in the post-treatment cells by Western blot analysis, tumor cells were washed with phosphate buffer saline (PBS), lysed with the radioimmunoprecipitation assay (RIPA) buffer (Pierce, Thermo Fisher), and separated with 10% SDS-PAGE gels (Biorad). Primary antibodies specific for HSP27 (Abcam), HSP70 (Cell Signaling Technologies), and HSP90 (Cell Signaling Technologies) were applied for analysis. To measure expression by quantitative real-time reverse transcription polymerase chain reaction (qRT-PCR), total RNA was extracted from ALDH1-positive tumor cells with the Trizol reagent (Life Technologies). The following primer sequences were used for PCR reactions: HSP27 (5′-TGGACCCCACCCAAGTTTC-3′, 5′-CGGCAGTCTCATCGGATTTT-3′); HSP70 (5′-CAAGATCAGCGAGGCCGA-3′, 5′-CCCTTGGGACCTGAGC-3′); and HSP90 (5′-AGAAATTGCCCAACTCATGTCC-3′, 5′-ATCAACTCCCGAAGGAAAATCTC-3′). mRNA levels were normalized to glyceraldehyde 3-phosphate dehydrogenase (GAPDH) and relative gene expression was calculated using the $2^{-\Delta\Delta CT}$ method [39]. Caspase-3 activity in ALDH1-positive cells was measured using a Colorimetric In-Cell enzyme-linked immunosorbent assay (ELISA) kit (Pierce) according to the manufacturer's instructions.

Particle biodistribution *in vivo* and intra-tumor temperature measurement

All mouse studies were performed in compliance with the guidelines of the Animal Welfare Act and the Guide for the Care and Use of Laboratory Animals following protocols approved by the Institutional Animal Care and Use Committee (IACUC) at Houston Methodist Research Institute. Biodistribution of AuPSMs in mice with orthotopic SUM159 tumors was determined based on silicon and gold contents using an inductively coupled-plasma optimal emission spectrometer (ICP-OES, Varian Inc). Briefly, 1×10^6 SUM159 cells in 0.1 mL PBS were inoculated in the mammary gland fat pad of 6-week-old female athymic nude mice. When tumor size reached 100 mm^3, the tumor-bearing mice were treated *i.v.* with 1×10^9 AuPSM, and euthanized 72 hours later. Organs were collected and their weights were recorded. To prepare samples for silicon content analysis, organs were homogenized in 1 mL 1N sodium hydroxide containing 20% ethanol, and incubated for 48 hours at room temperature. Tissue extracts were then centrifuged (400×g, 30 min), and 0.5 mL of the supernatant was diluted with 2.5 mL of deionized water. To prepare samples for gold content analysis, minced organs were digested in 0.5 mL aqua regia solution (nitric acid and hydrochloric acid, 1:3, v/v) for 72 hours. Samples were then diluted with 9.5 mL 2% nitric acid solution and centrifuged (400×g, 30 min). The values of gold and silicon obtained with ICP-OES measurement were then converted to percentage of injected dose per gram of tissue (%ID/g tissue).

To measure temperature changes inside the tumor, mice with SUM159 tumors in the mammary gland fat pads were treated *i.v.* with 1×10^9 AuPSM/mDTX particles. After 72 hours, the tumors were irradiated with a NIR laser at 1 W and 1.5 W for 5 min. A thermocouple (Oxford Optronix, Oxford, U. K.) inserted into the tumor was applied to record temperature changes.

Antitumor efficacy *in vivo*

Anti-tumor efficacy was investigated in female nude mice with orthotopic xenograft tumors from SUM159 cells. When tumor volume reached 150 mm^3, mice were randomly divided into 6 groups and treated with: 1) PBS, 2) PBS + NIR laser, 3) mDTX, 4) AuPSM/mDTX, 5) AuPSM + NIR laser, and 6) AuPSM/mDTX + NIR laser. mDTX was administered at a DTX-equivalent dose of 10 mg/kg, and AuPSMs were at 1×10^9 particles/mouse. NIR laser treatments (1.5 W output power, 5 min) were conducted three days after injection. Tumor volume and body weight were measured twice a week afterwards.

Mice with 4T1 orthotopic tumors were applied to assess tumor growth and lung metastasis. Briefly, 5×10^5 4T1 cells were inoculated into the 4th mammary fat pad of female Balb/c mice (6 week old, 18–20 g). When tumor volume reached 100 mm^3, mice were randomly divided into 6 groups (n = 8 mice/group), and treated with same regimens as in the SUM159 tumor model. Mice were monitored daily for tumor growth, and animals were euthanized when tumors became ulcerated or reached 1,500 mm^3. To evaluate 4T1 tumor lung metastasis, mice with 4T1 tumors received same treatments as described above, and were euthanized 4 weeks later. Number of metastatic nodules in the lung were counted, and tissue blocks were processed for hematoxylin and eosin (H&E) staining.

Stem cell activity and Western blot analysis in post-treatment mice

CSC activity was evaluated in post-treatment SUM159 tumors. Briefly, tumors were harvested 24 hours after irradiation and single-cell suspensions were obtained as described in the “mammosphere formation in cell culture” section. Single cells from primary mammospheres were seeded into 96-well ultra-low attachment plates and number of secondary mammospheres was counted seven days later. ALDH1 activity was measured with flow cytometry as described in the “cytotoxicity and ALDH1 activity assay *in vitro*” section. Human tumor cells were stained with an anti-human leukocyte antigen (HLA)-ABC antibody (BD Bioscience) and dead cells were detected with CYTOX® Blue (Life Technologies) staining.

Western blot analysis was performed with tumor and cell samples. To process tumor samples from post-treatment mice, tumors were harvested 24 hours after irradiation, minced, and lysed in RIPA buffer containing protease and phosphatase cocktail inhibitors. To process cells in CSC-rich mammospheres, RIPA buffer was added to primary mammospheres after 7 days in culture. Proteins were extracted and quantified using a Pierce BCA Protein Assay Kit (Thermo Scientific), and separated with 10% SDS-PAGE gels (Biorad). Primary antibodies specific for HSP27, HSP70 and HSP90 were applied for analysis using same antibodies as described in the “HSP expression analysis” section.

Statistical analysis

Statistical analyses were performed with the GraphPad Prism 5 software (GraphPad Software, Inc., CA). For all *in vitro* and *in vivo* analysis, sample sizes were chosen to ensure adequate power to detect a pre-specified effect size. P-values of less than 0.05 were considered statistically significant. Data are presented as means ± SD.

RESULTS

CSCs are sensitive to chemotherapy and mild hyperthermia combination treatment

The chemotherapy drug DTX is a standard-of-care treatment for TNBC. Our results indicate that both human TNBC cell lines, SUM159 and MDA-MB-231, were very sensitive to DTX treatment. The IC_{50} and IC_{90} DTX concentrations were 2 ng/mL and 10 ng/mL for SUM159 cells and 5 ng/mL and 20 ng/mL for MDA-MB-231 cells (Fig. 1A). Since ALDH1-positive cancer stem cells predict engraftment of primary breast tumors [40], we applied ALDH1 as the surrogate marker to track CSCs in this study. SUM159 and MDA-MB-231 cells contained 1.4% and 0.45% $ALDH1^+$ cells respectively, and DTX treatment caused a concentration-dependent increase in the proportion of $ALDH1^+$ cells (Fig. 1B). The level of $ALDH1^+$ cells was further confirmed in cells treated with the ALDH1-specific inhibitor DEAB (Fig. 1C). When treated with DTX at the IC_{90} concentrations, $ALDH1^+$cells increased by 3.7 and 3.6 folds in SUM159 and MDA-MB-231 cells respectively (Fig. 1B), indicating DTX treatment had enriched the $ALDH1^+$ cell population. $CD44^+/CD24^-/$ epithelial specific antigen $(ESA)^+$ are another panel of well-characterized surface markers for breast CSCs [37]. The $CD44^+/CD24^-/ESA^+$ cell population increased significantly following docetaxel treatment in both cell lines (Fig.S1 A-B). Since it was previously shown that CSCs were sensitive to hyperthermia [30], we isolated $ALDH1^+$ SUM159 and MDA-MB-231 cells by flow cytometry, treated them with DTX for 8 hours followed by a 5-minute incubation at 43ºC, and grew cells for another 24 hours to allow cells commit apoptosis. Dose-dependent increase in apoptotic cells were observed in both cell lines after they were co-treated with DTX and mild hyperthermia compared to cells in the DTX only treatment group (Fig. S1 C-D, Fig. 1D). The results demonstrate cooperative killing of CSCs by DTX and mild hyperthermia.

AuPSM serves both as a drug carrier and a generator of mild hyperthermia

PSMs with gold nanoparticle deposits (AuPSMs) were produced to serve as a carrier for chemotherapy drugs and a generator of mild hyperthermia. ICP-OES measurement detected 417 μg gold per billion AuPSMs. Microscopic analysis confirmed that gold nanoparticles with a medium diameter of 20 nm were deposited both on surface of PSM and inside the 40–100 nm pores (Fig.2A). The AuPSMs were then loaded with docetaxel micelles (mDTX) with an average size of 21 nm (Fig. 2B), with a final drug content of 200 μg DTX per billion AuPSMs. Spectrum scanning was applied to characterize absorption profiles of the particles (Fig. 2C). While the PSMs displayed a gradual decrease in absorbance in the 400–1,000 nm wavelength region and mDTX did not have a detectable level of absorbance across the whole spectrum, the AuPSM particles displayed a consistent high level of plasmon resonance absorbance throughout the visible light and near infrared (NIR) region (500–1,000 nm wavelength). Loading mDTX into AuPSM (AuPSM/mDTX) or simply mixing mDTX with AuPSM (AuPSM+mDTX) did not significantly change absorbance of the microparticles (Fig. 2C). Free AuPSM and AuPSM/mDTX, but not PSM, generated heat and raised temperature to 43–45°C in the solution when they were exposed to NIR laser at 810 nm for 10 min in water (Fig. 2D). PSMs with 20 nm gold nanoparticles were more efficient in heat generation than those with smaller particles, and the photothermal effect was repeatable upon NIR treatment (Fig. S2).

In vitro killing of SUM159 and MDA-MB-231 cells from AuPSM-loaded mDTX and mild hyperthermia was detected with live/dead cell staining (Fig. 2E). In SUM159 cells, treatment with AuPSM/mDTX or free mDTX for 72 hours caused about 40% cell death, and hyperthermia alone triggered 50% cell death. Combination of AuPSM and mild hyperthermia triggered 90% cell death. Similar pattern was observed with MDA-MD-231 cells, although these cells were more sensitive to mDTX and less sensitive to hyperthermia than SUM159 cells (Fig. 2F). The results indicate effective killing of breast cancer cells by combination of chemotherapy and hyperthermia.

Chemo-mild hyperthermia combination inhibits CSC activity.

Mammosphere formation in growth factor-supplemented suspension has previously been used to enrich stem/progenitor cells from primary breast cancer tissues and to evaluate self-renewal capacity and tumorigenicity of CSCs [41, 42]. We applied the mammosphere assay to test the effects of chemo-mild hyperthermia combination on the self-renewal of therapy-resistant CSCs. Tumor cells isolated from primary SUM159 and MDA-MB-231 xenograft tumors were capable of forming mammospheres when seeded in ultra-low attachment plates (data not shown). We digested the primary mammospheres, seeded single cells back onto ultra-low attachment plates, and treated them with mDTX, AuPSM, or AuPSM/mDTX for 3 days followed by mild hyperthermia. The post-treatment cells were allowed to grow 7 more days for mammosphere formation. While mDTX or mild hyperthermia single treatment inhibited mammosphere formation, it was the combination treatment that significantly reduced the number of mammospheres (Fig.3), demonstrating cooperative effects between mDTX and mild hyperthermia on inhibition of CSC self-renewal capability.

DTX treatment sensitizes CSCs to mild hyperthermia by inhibiting HSP27 expression.

SUM159 and MDA-MB-231 cells were treated with DTX, and potential involvement of HSPs in mediating cellular response was investigated. Interestingly, drug treatment triggered a dramatic reduction in HSP27 protein levels at the IC_{90} levels (10 and 20 ng/mL for SUM159 and MDA-MB-231, respectively), but left HSP70 and HSP90 protein levels unchanged (Fig.4A). We isolated $ALDH1^+$ cancer cells from post-treatment samples, and performed gene expression analysis. Quantitative RT-PCR analysis of the SUM159 samples revealed that treatment with 10 ng/mL, but not 2 ng/mL, decreased *HSP27* mRNA expression. Upon treatment with mild hyperthermia, *HSP27* mRNA increased by 2 folds in cells pretreated with 2 ng/mL DTX; however, there was no increase in *HSP27* mRNA level in cells treated with 10 ng/mL DTX (Fig. 4B). Similar pattern was also observed in $ALDH1^+$ MDA-MB-231 and 4T1cells (Fig.S3A-C). In both cases, treatment of cells with docetaxel at the IC_{90} concentration (20 ng/mL for MDA-MB-231 and 80 ng/mL for 4T1) suppressed HSP27 or the human homologue of the murine protein (HSP25) expression. In $ALDH1^+$ MDA-MB-231 cells with overexpression of the multi-drug resistance gene (MDA-MB-231/MDR), docetaxel concentrations at both the IC_{50} and IC_{90} levels (90 and 380 ng/mL, respectively) were able to suppress hyperthermia-induced Hsp27 expression was suppressed by docetaxel at both IC_{50} and IC_{90} concentrations (Fig.S3D-E). To determine whether HSP27 played a critical role on resistance to mild hyperthermia, we transfected SUM159 cells with *HSP27* gene-specific siRNA oligos and treated cells with mild hyperthermia, and confirmed knockdown of HSP27 by Western blot analysis (Fig. 4C).

While inhibition of HSP27 alone did not cause significant level of cell death in ALDH1$^+$ cells, co-treatment of the cells with mild hyperthermia induced a 3-fold increase in cell death, a level that was significantly higher than in cells transfected with a control scramble siRNA and treated with mild hyperthermia (Fig. 4D). To confirm further the essential role of HSP27 in therapy resistance, we stably overexpressed HSP27 in SUM159 cells (Fig. 4E) and treated cells with DTX and mild hyperthermia. HSP27 overexpression reversed apoptosis induced by the DTX-mild hyperthermia combination in ALDH1$^+$ cells, as indicated by the significant decrease in caspase 3 activity (Fig. 4F). These studies indicate that DTX treatment-induced HSP27 reduction plays an essential role in sensitizing breast CSCs to mild hyperthermia.

DTX-mild hyperthermia combination treatment effectively inhibits tumor growth.

We have previously applied PSM-based platforms to deliver therapeutic agents for cancer treatment, and demonstrated the effectiveness of such platforms in overcoming biological barriers [42–46]. In this study, we treated mice carrying SUM159 orthotopic tumors with 1×10^9 AuPSM particles, and confirmed tumor accumulation of AuPSM particles based on both silicon and gold content analysis (Fig. 5A). NIR irradiation at a laser output power of 1.5 watts triggered an intra-tumoral temperature increase to 45ºC within 5 minutes (Fig. 5B). Based on DTX loading capacity (200 μg DTX/1×10^9 AuPSM), tumor accumulation (Fig. 5A) and proper heat generation capability (Fig. 5B), we fixed AuPSM and AuPSM/mDTX at 1×10^9 particles per mouse for *in vivo* dosing. To evaluate therapeutic efficacy, mice with primary SUM159 tumors were first treated *i.v.* with mDTX, AuPSM or AuPSM/mDTX when the tumors reached 150 mm^3 and then with mild hyperthermia 3 days later. Based on our previous studies, we expected that over 50% of the drug particles has been released from the carrier 3 days after treatment. As expected, mDTX treatment only partially inhibited tumor growth compared to the mock treatment control group. AuPSM/mDTX treatment was more efficacious than mDTX in the first 2 weeks, but tumor growth resumed afterwards, and tumor growth in the mild hyperthermia treatment growth (AuPSM+laser) displayed a similar pattern (Fig. 5C). In contrast, mice in the chemo-mild hyperthermia combination group (AuPSM/mDTX+laser) displayed complete inhibition of tumor growth inhibition for the next 3 weeks (Fig. 5C).

Therapeutic benefit from chemo-mild hyperthermia combination was also evaluated in the murine 4T1 mammary gland tumor model. Mice with primary 4T1 tumors were treated with the same regimens as in the SUM159 tumor study, and tumor metastasis to the lung was evaluated. While treatment with mDTX or AuPSM/mDTX or mild hyperthermia alone did not significantly reduce number of tumor nodules in the lung comparing to the PBS control group, combination of AuPSM/mDTX and mild hyperthermia caused dramatic reduction in lung metastatic nodes (Fig. 5D). In addition, tumor nodules in the combination treatment group were also much smaller than those in the single treatment groups (Fig. 5E). In a separate study, we assessed survival benefit from single or combination treatments. Mice in PBS and PBS+laser treatment groups died 25 ~ 33 days after tumor cell inoculation. Treatment with mDTX, AuPSM/mDTX or AuPSM+laser provided moderate but statistically significant survival benefit over the PBS control group. The most significant survival benefit was obtained in mice treated with AuPSM/mDTX+laser, with a median survival time of 45.5

days (Fig. 5F). Thus, the chemo-mild hyperthermia combination treatment is superior over single treatments.

DTX-mild hyperthermia combination treatment significantly reduces CSC population within the tumor

To confirm the impact of chemo-mild hyperthermia combination treatment on CSCs *in vivo*, we treated SUM159 orthotopic tumors and isolated single tumor cells 24 hours after mild hyperthermia treatment to measure CSC numbers and activity. Percentage of $ALDH1^+$ cells increased moderately in the mDTX and AuPSM/mDTX treatment groups (11.8% and 10.6%) compared to the PBS control group (9.57%), but decreased by 52% (to 4.68%) in the mild hyperthermia treatment group, and further decreased by another 46% (to 2.50%) in the chemo-mild hyperthermia combination treatment group (Fig. 6A-B). Mammosphere assay results correlated with the cell population analysis data (Fig. 6C) and demonstrated a significant reduction of CSC activity in cells isolated from the combination treatment group over the DTX alone or mild hyperthermia treatment alone group. Western blot analysis revealed elevated expression levels of HSP27, HSP 70 and HSP90 after mild hyperthermia treatment, and mDTX treatment dramatically reduced expression of HSP27, but not HSP70 or HSP90, in both whole tumor lysates and cells prepared from mammospheres (Fig. 6D). Taken together, results indicate that chemo-mild hyperthermia combination treatment eliminates CSCs and inhibits TNBC tumor growth and metastasis.

DISCUSSION

Mounting evidence indicates persistent existence of CSCs after chemotherapy and radiation therapy [47]. Developing new treatments to eliminate CSC holds the key to success in the fight against human cancers. In the current study, we detected preferential killing of non-CSC TNBC cells in culture by DTX which is one of the most commonly used chemotherapeutic agents in the treatment of breast cancer, resulting in enrichment of the $ALDH1^+$ CSCs. Based on the observation that DTX and mild hyperthermia combination treatment could synergistically trigger CSC apoptosis, we developed a PSM-based platform to enable concurrent application of chemotherapy and mild hyperthermia to the same cancer cells *in vivo*. Porous silicon particles are degradable and biocompatible [35, 44]. We have previously applied porous silicon particles as the carrier to deliver small molecule drugs and therapeutic siRNA/microRNA to tumor tissues and demonstrated superb therapeutic efficacy and lack of toxicity from the carrier in animal tumor models [42–46, 48, 49]. The systemically injected discoidal PSM particles preferentially attach to the surface of tumor vasculature, and the cargos are slowly unloaded from the carrier when porous silicon gradually dissolves in the body fluid [48]. Since there exist multiple physical and biological barriers inside the body to block effective drug accumulation into the tumor tissues [28], these particles can also be conjugated with affinity targeting moieties on surface so as to effectively deliver drug molecules to the CSC niches [19, 50]. Depositing gold nanoparticles in the confinement of nanopores inside PSM has the benefit of concomitant particle stimulation by NIR, as we have demonstrated previously [51].

It has been well documented that the microtubule-targeting agents, including DTX, induce cell death through mitotic arrest [52, 53]. However, cancer cells may recover from mitotic arrest when chemotherapeutic drugs are present in low concentrations [54]. In this study, we packaged DTX molecules in polymeric micelles and loaded them into the nanopores of PSM. The resulting AuPSM/mDTX provides at least two levels of benefit in cancer treatment: 1) sustained local drug release from PSM and 2) effective particulate drug penetration into the tumor taking advantage of the enhanced permeability and retention effect of the leaky tumor vasculature [55, 56]. Notably, we did not assess the clearance of mDTX *in vivo* by measuring drug concentrations in serum and urine. Prior to considering translation into clinical applications, the clearance of DTX utilizing this platform would need to be quantified in future studies.

An interesting but surprising observation was that DTX treatment caused dramatic reduction of HSP27 level in TNBC cells. Among the list of overexpressed HSPs triggered by hyperthermia as a result of stress response [31], HSP27 has a unique role on CSC activity. It has been reported that HSP27 phosphorylation is enhanced in $ALDH1^+$ breast cancer CSCs [57], and that the protein is absolutely essential for CSC activity in multiple cancer types [32–34]. There have also been multiple efforts to develop HSP27-targeted cancer therapeutics [58]. Thus, in addition to killing the bulk of non-CSC cancer cells, DTX contributes to CSC killing by suppressing HSP27 expression. This constitutes a novel mechanism of action of AuPSM/mDTX in killing breast cancer CSCs in this study.

These findings could have noteworthy clinical applications with modification and additional studies. Although one limitation of this treatment mechanism is the penetration depth of NIR to ensure adequate power for heat generation depending on the tissue depth of breast tumors relative to the NIR source, many primary breast tumors are relatively superficial. Furthermore, alternate techniques could be utilized for delivering NIR such as placing the laser probe within the tumor itself [59]. Neoadjuvant treatment with AuPSM/mDTX and NIR to cause hyperthermia could prevent metastases by killing those cells in the primary tumor that will develop into CSCs prior to surgical resection. Additional studies would be needed to investigate the ability of this platform to kill CSCs and non-CSCs utilizing a milder hyperthermia (<43°C) that would: 1) minimize thermal injury to surrounding breast tissue and dermis and 2) not be painful to patients, so as to avoid the risk, expense, and inconvenience of treatment under general anesthesia [60]. In addition, future studies must address off-target effects including non-targeted drug accumulation, potential side effects, and altered clearance resulting from our novel therapeutic platform.

In conclusion, we have developed AuPSM/mDTX as a novel therapeutic agent to treat TNBC. AuPSM/mDTX kills cancer cells through sustained release of DTX micelles and generation of mild hyperthermia. DTX-mediated suppression of HSP27 synergizes CSC killing by mild hyperthermia. Future studies will need to evaluate the effect of docetaxel on HSP27 in other tumor types and whether synergistic cytotoxicity with mild hyperthermia is observed. Given the broad applicability of our microparticle platform for drug delivery and dual therapy with nanoparticle-mediated mild hyperthermia, this approach could be replicated to provide delivery of the powerful combination of chemotherapy and thermotherapy to kill cancer stem-like cells in multiple types and sites.

Supplementary Material

Refer to Web version on PubMed Central for supplementary material.

Acknowledgments

Financial Support: The authors acknowledge financial support from the following sources: National Cancer Institute **(**1R01CA193880, U54CA143837 and U54CA210181), Department of Defense (W81XWH-12-1-0414), National Natural Science Foundation of China (81703713), Key project of Wenzhou Institute of Biomaterials & Engineering (WIBEZD2017001-03), and the Ernest Cockrell Jr. Presidential Distinguished Chair.

REFERENCES

1. Foulkes WD, Smith IE, and Reis JS, Triple-Negative Breast Cancer. New England Journal of Medicine, 2010 363(20): p. 1938–1948. [PubMed: 21067385]
2. Bianchini G, et al., Triple-negative breast cancer: challenges and opportunities of a heterogeneous disease. Nat Rev Clin Oncol, 2016 13(11): p. 674–690. [PubMed: 27184417]
3. Idowu MO, et al., CD44(+)/CD24(-/low) cancer stem/progenitor cells are more abundant in triple-negative invasive breast carcinoma phenotype and are associated with poor outcome. Hum Pathol, 2012 43(3): p. 364–73. [PubMed: 21835433]
4. McDermott SP and Wicha MS, Targeting breast cancer stem cells. Mol Oncol, 2010 4(5): p. 404–19. [PubMed: 20599450]
5. Al-Hajj M, et al., Prospective identification of tumorigenic breast cancer cells. Proc Natl Acad Sci U S A, 2003 100(7): p. 3983–8. [PubMed: 12629218]
6. Tang DG, Understanding cancer stem cell heterogeneity and plasticity. Cell Res, 2012 22(3): p. 457–72. [PubMed: 22357481]
7. Visvader JE and Lindeman GJ, Cancer stem cells in solid tumours: accumulating evidence and unresolved questions. Nat Rev Cancer, 2008 8(10): p. 755–68. [PubMed: 18784658]
8. Shibue T and Weinberg RA, EMT, CSCs, and drug resistance: the mechanistic link and clinical implications. Nat Rev Clin Oncol, 2017.
9. Li X, et al., Intrinsic resistance of tumorigenic breast cancer cells to chemotherapy. J Natl Cancer Inst, 2008 100(9): p. 672–9. [PubMed: 18445819]
10. Ishikawa F, et al., Chemotherapy-resistant human AML stem cells home to and engraft within the bone-marrow endosteal region. Nat Biotechnol, 2007 25(11): p. 1315–21. [PubMed: 17952057]
11. Yu F, et al., let-7 regulates self renewal and tumorigenicity of breast cancer cells. Cell, 2007 131(6): p. 1109–23. [PubMed: 18083101]
12. Schatton T, et al., Identification of cells initiating human melanomas. Nature, 2008 451(7176): p. 345–9. [PubMed: 18202660]
13. Bao S, et al., Glioma stem cells promote radioresistance by preferential activation of the DNA damage response. Nature, 2006 444(7120): p. 756–60. [PubMed: 17051156]
14. Nguyen LV, et al., Cancer stem cells: an evolving concept. Nat Rev Cancer, 2012 12(2): p. 133–43. [PubMed: 22237392]
15. Yen WC, et al., Targeting Notch Signaling with a Notch2/Notch3 Antagonist (Tarextumab) Inhibits Tumor Growth and Decreases Tumor-Initiating Cell Frequency. Clinical Cancer Research, 2015 21(9): p. 2084–2095. [PubMed: 25934888]
16. Zheng FM, et al., A Novel Small Molecule Aurora Kinase Inhibitor Attenuates Breast Tumor-Initiating Cells and Overcomes Drug Resistance. Molecular Cancer Therapeutics, 2014 13(8): p. 1991–2003. [PubMed: 24899685]
17. Janzer A, et al., Metformin and phenformin deplete tricarboxylic acid cycle and glycolytic intermediates during cell transformation and NTPs in cancer stem cells. Proceedings of the National Academy of Sciences of the United States of America, 2014 111(29): p. 10574–10579. [PubMed: 25002509]

18. Saha S, et al., Aspirin suppresses the acquisition of chemo-resistance in breast cancer by disrupting an NFkappaB-IL6 signaling axis responsible for the generation of cancer stem cells. Cancer Res, 2016.
19. Zong H, et al., In vivo targeting of leukemia stem cells by directing parthenolide-loaded nanoparticles to the bone marrow niche. Leukemia, 2016 30(7): p. 1582–6. [PubMed: 26669973]
20. Hambardzumyan D, et al., PI3K pathway regulates survival of cancer stem cells residing in the perivascular niche following radiation in medulloblastoma in vivo. Genes Dev, 2008 22(4): p. 436–48. [PubMed: 18281460]
21. Singh SK, et al., Identification of human brain tumour initiating cells. Nature, 2004 432(7015): p. 396–401. [PubMed: 15549107]
22. O'Brien CA, et al., A human colon cancer cell capable of initiating tumour growth in immunodeficient mice. Nature, 2007 445(7123): p. 106–10. [PubMed: 17122772]
23. Ricci-Vitiani L, et al., Identification and expansion of human colon-cancer-initiating cells. Nature, 2007 445(7123): p. 111–5. [PubMed: 17122771]
24. Ginestier C, et al., ALDH1 is a marker of normal and malignant human mammary stem cells and a predictor of poor clinical outcome. Cell Stem Cell, 2007 1(5): p. 555–67. [PubMed: 18371393]
25. Jin L, et al., Targeting of CD44 eradicates human acute myeloid leukemic stem cells. Nat Med, 2006 12(10): p. 1167–74. [PubMed: 16998484]
26. Krause DS, et al., Requirement for CD44 in homing and engraftment of BCR-ABL-expressing leukemic stem cells. Nat Med, 2006 12(10): p. 1175–80. [PubMed: 16998483]
27. Merino VF, et al., Combined Treatment with Epigenetic, Differentiating, and Chemotherapeutic Agents Cooperatively Targets Tumor-Initiating Cells in Triple-Negative Breast Cancer. Cancer Res, 2016 76(7): p. 2013–2024. [PubMed: 26787836]
28. Blanco E, Shen H, and Ferrari M, Principles of nanoparticle design for overcoming biological barriers to drug delivery. Nat Biotechnol, 2015 33(9): p. 941–51. [PubMed: 26348965]
29. Maier-Hauff K, et al., Intracranial thermotherapy using magnetic nanoparticles combined with external beam radiotherapy: results of a feasibility study on patients with glioblastoma multiforme. J Neurooncol, 2007 81(1): p. 53–60. [PubMed: 16773216]
30. Atkinson RL, et al., Thermal enhancement with optically activated gold nanoshells sensitizes breast cancer stem cells to radiation therapy. Sci Transl Med, 2010 2(55): p. 55-79.
31. Fisher JW, et al., Photothermal response of human and murine cancer cells to multiwalled carbon nanotubes after laser irradiation. Cancer Res, 2010 70(23): p. 9855–64. [PubMed: 21098701]
32. Sakurai T, et al., p38alpha inhibits liver fibrogenesis and consequent hepatocarcinogenesis by curtailing accumulation of reactive oxygen species. Cancer Res, 2013 73(1): p. 215–24. [PubMed: 23271722]
33. Lin SP, et al., Survival of cancer stem cells under hypoxia and serum depletion via decrease in PP2A activity and activation of p38-MAPKAPK2-Hsp27. PLoS One, 2012 7(11): p. e49605. [PubMed: 23185379]
34. Straume O, et al., Suppression of heat shock protein 27 induces long-term dormancy in human breast cancer. Proc Natl Acad Sci U S A, 2012 109(22): p. 8699–704. [PubMed: 22589302]
35. Godin B, et al., Discoidal Porous Silicon Particles: Fabrication and Biodistribution in Breast Cancer Bearing Mice. Adv Funct Mater, 2012 22(20): p. 4225–4235. [PubMed: 23227000]
36. Mu CF, et al., The effects of mixed MPEG-PLA/Pluronic copolymer micelles on the bioavailability and multidrug resistance of docetaxel. Biomaterials, 2010 31(8): p. 2371–9. [PubMed: 20031202]
37. McClements L, et al., Targeting Treatment-Resistant Breast Cancer Stem Cells with FKBPL and Its Peptide Derivative, AD-01, via the CD44 Pathway. Clinical Cancer Research, 2013 19(14): p. 3881–3893. [PubMed: 23741069]
38. Kumano M, et al., Cotargeting Stress-Activated Hsp27 and Autophagy as a Combinatorial Strategy to Amplify Endoplasmic Reticular Stress in Prostate Cancer. Molecular Cancer Therapeutics, 2012 11(8): p. 1661–1671. [PubMed: 22675041]
39. Livak KJ and Schmittgen TD, Analysis of relative gene expression data using real-time quantitative PCR and the 2(T)(-Delta Delta C) method. Methods, 2001 25(4): p. 402–408. [PubMed: 11846609]

40. Charafe-Jauffret E, et al., ALDH1-positive cancer stem cells predict engraftment of primary breast tumors and are governed by a common stem cell program. Cancer Res, 2013 73(24): p. 7290–300. [PubMed: 24142344]
41. Debeb BG, et al., Histone deacetylase inhibitors stimulate dedifferentiation of human breast cancer cells through WNT/beta-catenin signaling. Stem Cells, 2012 30(11): p. 2366–77. [PubMed: 22961641]
42. Dave B, et al., Targeting RPL39 and MLF2 reduces tumor initiation and metastasis in breast cancer by inhibiting nitric oxide synthase signaling. Proc Natl Acad Sci U S A, 2014 111(24): p. 8838–43. [PubMed: 24876273]
43. Shen H, et al., Enhancing chemotherapy response with sustained EphA2 silencing using multistage vector delivery. Clin Cancer Res, 2013 19(7): p. 1806–15. [PubMed: 23386691]
44. Xu R, et al., Multistage Vectored siRNA Targeting Ataxia-Telangiectasia Mutated for Breast Cancer Therapy. Small, 2013 9(9–10): p. 1799–808. [PubMed: 23293085]
45. Zhang M, et al., Polycation-functionalized nanoporous silicon particles for gene silencing on breast cancer cells. Biomaterials, 2014 35: p. 423–431. [PubMed: 24103653]
46. Shen J, et al., High capacity nanoporous silicon carrier for systemic delivery of gene silencing therapeutics. ACS Nano, 2013 7(11): p. 9867–80. [PubMed: 24131405]
47. Kreso A and Dick JE, Evolution of the cancer stem cell model. Cell Stem Cell, 2014 14(3): p. 275–91. [PubMed: 24607403]
48. Xu R, et al., An injectable nanoparticle generator enhances delivery of cancer therapeutics. Nat Biotechnol, 2016 34(4): p. 414–8. [PubMed: 26974511]
49. Ban Y, et al., Targeting Autocrine CCL5-CCR5 Axis Reprograms Immunosuppressive Myeloid Cells and Reinvigorates Antitumor Immunity. Cancer Res, 2017 77(11): p. 2857–2868. [PubMed: 28416485]
50. Mai J, et al., Bone marrow endothelium-targeted therapeutics for metastatic breast cancer. J Control Release, 2014 187: p. 22–9. [PubMed: 24818768]
51. Shen H, et al., Cooperative, nanoparticle-enabled thermal therapy of breast cancer. Adv Healthc Mater, 2012 1(1): p. 84–9. [PubMed: 23184690]
52. Hernandez-Vargas H, Palacios J, and Moreno-Bueno G, Molecular profiling of docetaxel cytotoxicity in breast cancer cells: uncoupling of aberrant mitosis and apoptosis. Oncogene, 2007 26(20): p. 2902–13. [PubMed: 17099726]
53. Jordan MA and Wilson L, Microtubules as a target for anticancer drugs. Nat Rev Cancer, 2004 4(4): p. 253–65. [PubMed: 15057285]
54. Morse DL, et al., Docetaxel induces cell death through mitotic catastrophe in human breast cancer cells. Mol Cancer Ther, 2005 4(10): p. 1495–504. [PubMed: 16227398]
55. Matsumura Y and Maeda H, A new concept for macromolecular therapeutics in cancer chemotherapy: mechanism of tumoritropic accumulation of proteins and the antitumor agent smancs. Cancer Res, 1986 46(12 Pt 1): p. 6387–92. [PubMed: 2946403]
56. Maeda H, Toward a full understanding of the EPR effect in primary and metastatic tumors as well as issues related to its heterogeneity. Adv Drug Deliv Rev, 2015 91: p. 3–6. [PubMed: 25579058]
57. Wei L, et al., Hsp27 participates in the maintenance of breast cancer stem cells through regulation of epithelial-mesenchymal transition and nuclear factor-kappaB. Breast Cancer Res, 2011 13(5): p. R101. [PubMed: 22023707]
58. Hendriks LEL and Dingemans AC, Heat shock protein antagonists in early stage clinical trials for NSCLC. Expert Opin Investig Drugs, 2017 26(5): p. 541–550.
59. Hudson DE, et al., Penetration of laser light at 808 and 980 nm in bovine tissue samples. Photomed Laser Surg, 2013 31(4): p. 163–8. [PubMed: 23441909]
60. Ungar E and Stroud K, A New Approach to Defining Human Touch Temperature Standards, in 40th International Conference on Environmental Systems. 2010, American Institute of Aeronautics and Astronautics

Statement of Significance:

The current study offers a novel approach to eliminate therapy-resistant cells in breast cancer and uncovers the underlying mechanism of action.

STATEMENT OF TRANSLATIONAL RELEVANCE

Conventional chemotherapy cannot effectively eliminate every cancer cell in a tumor. The small population of therapy-resistant cells is responsible for tumor recurrence and metastasis. We have developed a multidisciplinary approach to concurrently kill both the bulk of cancer cells and therapy-resistant cells. This approach is expected to significantly improve therapy outcome.

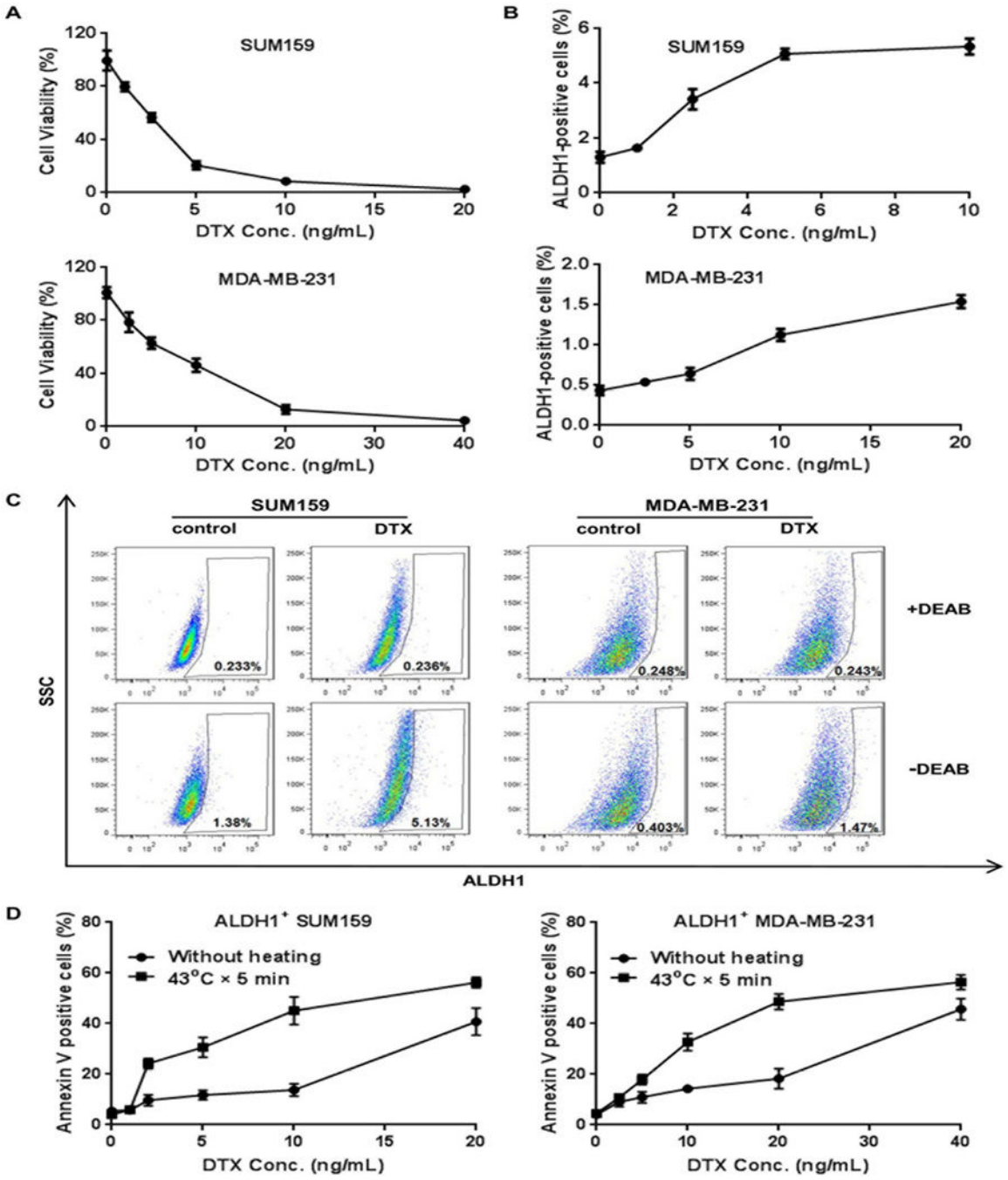

Fig. 1. Synergistic killing of CSCs by docetaxel and mild hyperthermia.

(A) Dose-dependent killing of human breast cancer cells. SUM159 and MDA-MB-231 cells were treated with increasing concentrations of DTX for 72 hours, and cell viability was measured with the MTT assay. (B) Dose-dependent enrichment of CSCs. Flow cytometry analysis was performed to measure ALDH1-positive cells after 72 hour DTX treatment. (C) Representative images of flow cytometry analysis of cells treated with or without DEAB in the ALDH1 staining buffer following treatment with DTX at IC_{90} concentration. (D) Analysis of apoptotic ALDH1-positive SUM159 and MDA-MB-231 cells 24 hours after

cells were treated with DTX for 8 hours followed by hyperthermia at 43°C for 5 min. The mean and standard deviations were calculated from three replicates.

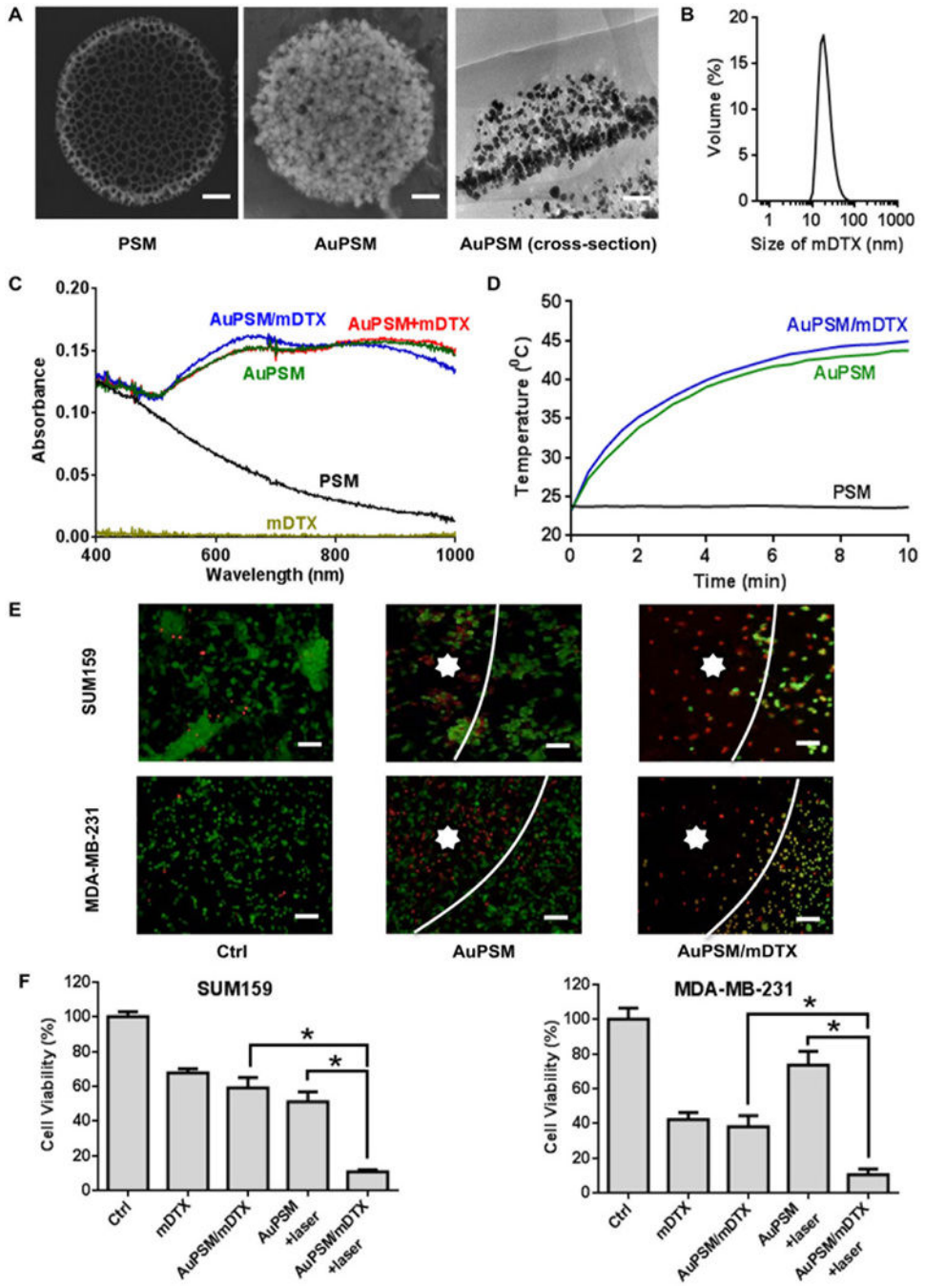

Fig. 2. Characterization of the porous silicon microparticle-based platform and assessment of *in vitro* cell killing.

(A) Images of PSM and AuPSM. Left panel: SEM image of PSM; middle panel: SEM image of AuPSM; right panel: TEM image of AuPSM. Scale bar in SEM images: 100 nm. (B) Size distribution of DTX micelles (mDTX). (C) Ultraviolet-visible spectroscopy (UV-Vis) absorption spectra of mDTX, PSM, AuPSM, AuPSM/mDTX, and a simple mix of AuPSM and mDTX (AuPSM+mDTX). (D) Time-dependent heat generation after the PSM, AuPSM and AuPSM/mDTX particles were treated with NIR. Temperature changes were measured during NIR treatment at a wavelength of 810 nm. (E) Fluorescent microscopic

images of post-treatment SUM159 and MDA-MB-231 breast cancer cells. Cells were treated with AuPSM or AuPSM/mDTX for 72 hours followed by NIR irradiation. They were stained with calcein AM for live cells (in green) and EthD-1 for dead cells (in red). White line: the boundary between irradiation and non-irradiation areas. Star: irradiated area. Scale bar: 100 μm. (F) SUM159 and MDA-MB-231 cell viability after cells were treated for 72 hours with mDTX (2 ng/mL DTX for SUM159 cells and 10 ng/mL DTX for MDA-MB-231 cells) followed by NIR irradiation. Results represent mean ± SD of four replicates. Ctrl: no treatment control. *, $p < 0.05$.

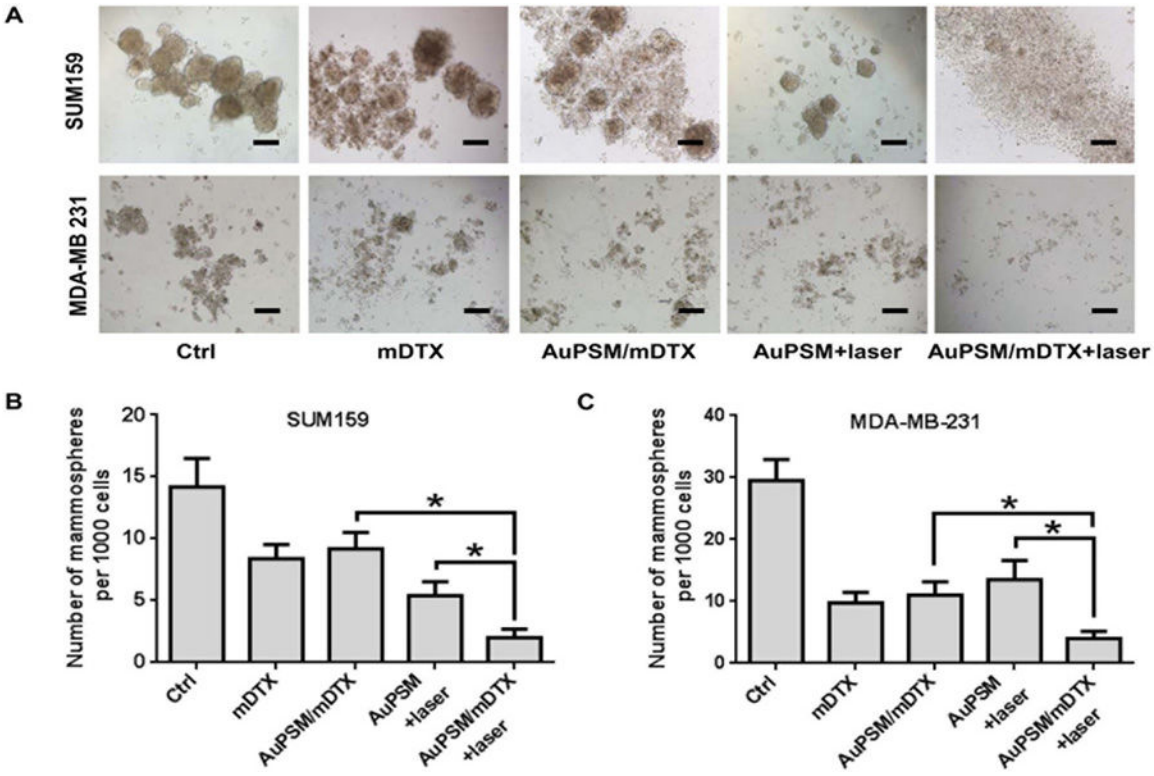

Fig. 3. Measurement of CSC activity based on mammosphere formation.

Cells isolated from primary SUM159 and MDA-MB-231 tumors were treated with mDTX and/or mild hyperthermia, and seeded in low attachment plates for mammosphere formation. (A) Representative images of SUM159 and MDA-MB-231 mammospheres 7 days after seeding. Scale bar: 100 μm. (B) Quantitative analysis of SUM159 mammospheres. (C) Quantitative analysis of MDA-MB-231 mammospheres from triplicate experiments. *, $p < 0.05$.

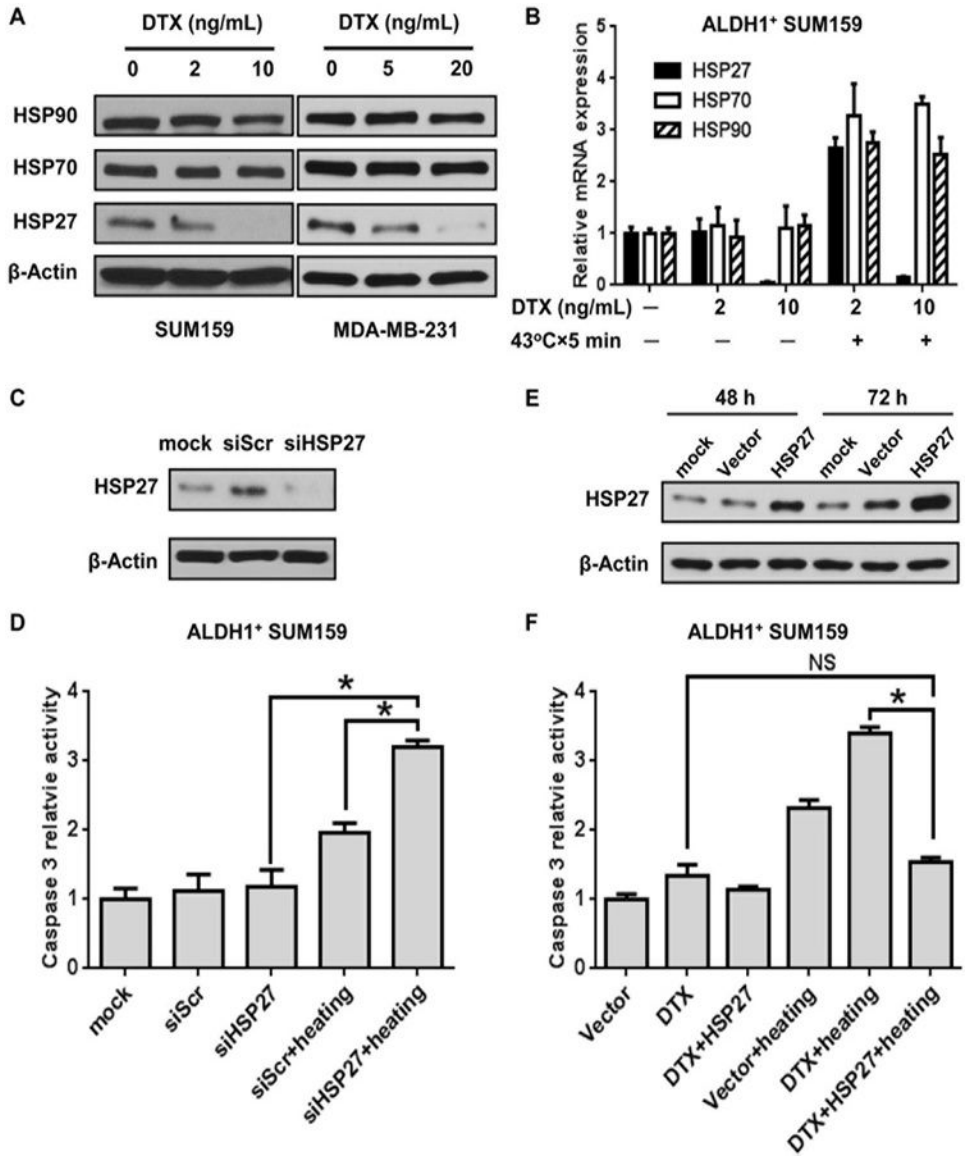

Fig. 4. Determination of HSP27 contribution on CSC viability.

(A) Western blot analysis on HSP27, HSP70 and HSP90 expression in SUM159 and MDA-MB-231 cells after DTX treatment for 8 hours. β-Actin served as control for equal protein loading. (B) Quantitative RT-PCR analysis of HSP27, HSP70 and HSP90 mRNA levels in ALDH1-positive SUM159 cells after treatment with DTX for 8 hours followed by mild hyperthermia at 43°C for 5 min. (C) Western blot analysis on knockdown of HSP27 expression in SUM159 cells treated with a scramble control siRNA (siScr) or a gene-specific siRNA (siHSP27). (D) Quantitative analysis of caspase 3 activity in ALDH1-positive SUM159 cells after the siScr or siHSP27-transfected cells were treated with mild hyperthermia at 43°C for 5 min. The data are the mean and SD of four replicates. *, $p < 0.05$. (E) Western blot analysis on HSP27 overexpression in SUM159 cells transfected with an empty pCMV6-Entry control plasmid (Vector) or a pCMV6-Entry/HSPB1 plasmid carrying the HSP27 gene. β-Actin served as a control for equal protein loading. (F)

Quantitative analysis of caspase 3 activity in ALDH1-positive SUM159 cells after the transfected cells were treated with DTX for 8 hours followed by mild hyperthermia at 43°C for 5 min. Error bars indicate the standard deviations of the average values from four replicates. *, $p < 0.05$.

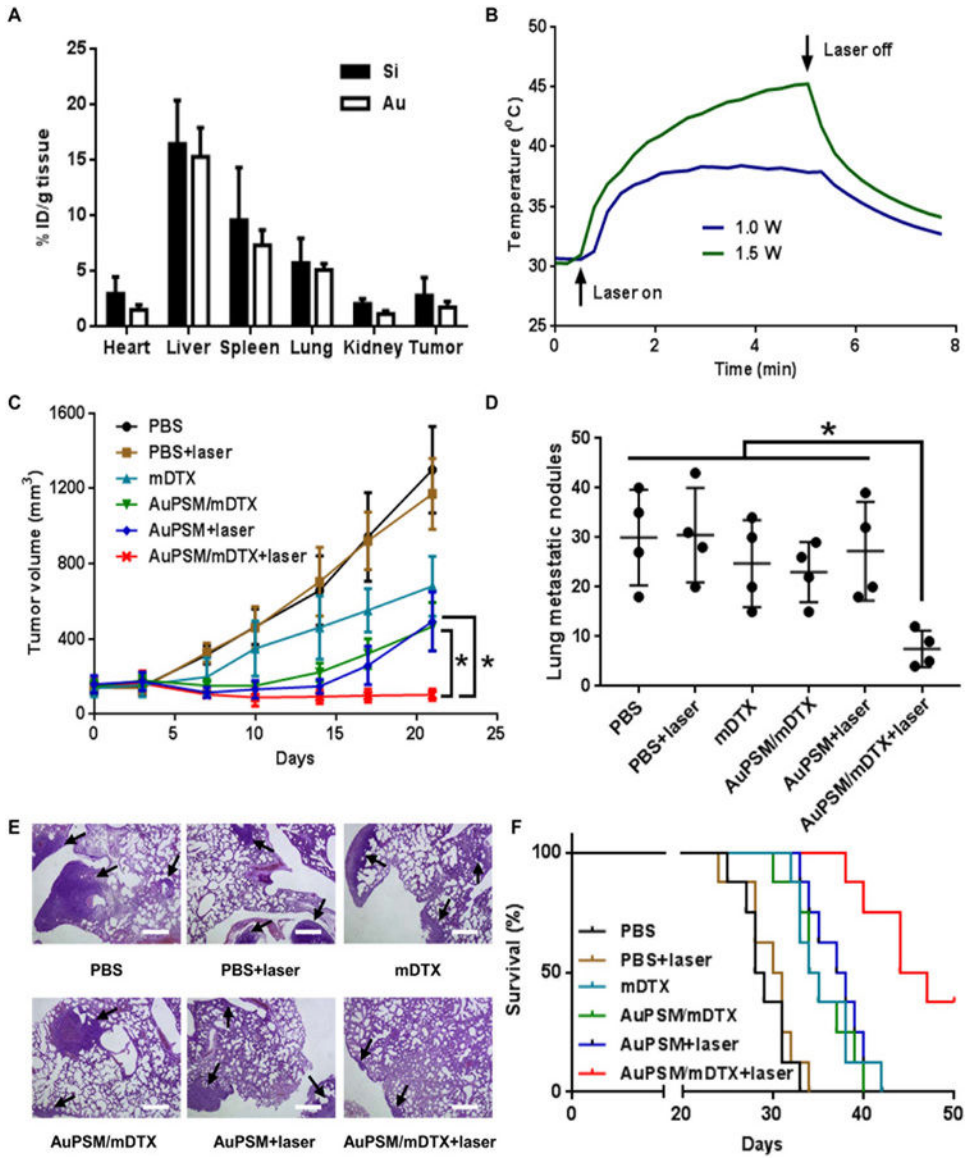

Fig. 5. Evaluation of therapeutic efficacy from AuPSM/mDTX.

(A) Biodistribution of AuPSM. Nude mice with primary SUM159 tumors were treated *i.v.* with 1×10^9 AuPSM particles per mouse. They were sacrificed 72 hours later, particle biodistribution was analyzed in major organs and the tumor tissue based on silicon (Si) and gold (Au) content. (B) Intra-tumoral temperature changes after NIR treatment. Nude mice with primary SUM159 tumors were treated *i.v.* with 1×10^9 AuPSM particles per mouse and then treated with NIR at two different powers. Time-dependent temperature change was recorded and plotted. (C) Time-dependent SUM159 primary tumor growth in post-treatment mice (n = 6 mice/group). (D) Analysis of lung metastatic tumor nodules in BALB/c mice with primary 4T1 tumors after single agent or combination treatment (n = 4). (E) Representative images of metastatic 4T1 tumor nodules in the lung after H&E staining. Tumor nodules are pointed with black arrows. (F) Kaplan–Meier plot of BALB/c mice with primary 4T1 tumors after single agent or combination treatment (n = 8 mice/group).

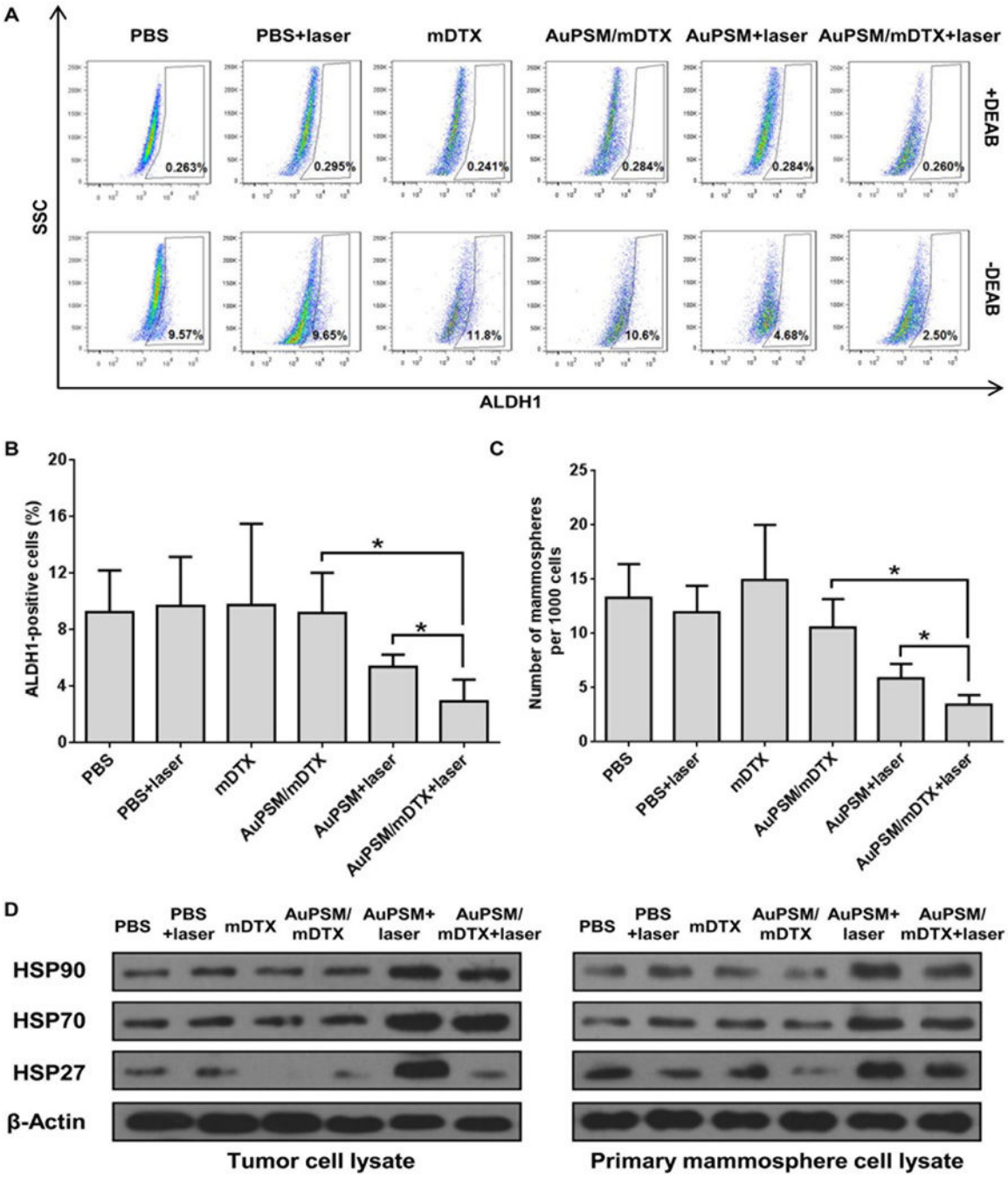

Fig.6. CSC analysis in post-treatment tumor samples.

Nude mice with primary SUM159 tumors were sacrificed 24 hours after NIR treatment, and tumor samples were collected to isolate single cells for CSC assay. (A) Representative flow cytometry graphs of ALDH1 assay. SSC: side scatter. (B) Summary of ALDH1-positive cells in post-treatment tumor tissue. Results represent mean ± SD (n = 4 mice/group). (C) Summary of mammosphere formation from post-treatment tumor cells. The mean and standard deviations were calculated from four replicates. *, $p < 0.05$. (D) Western blot

analysis on protein expression in SUM159 tumor samples harvested 24 hours after treatment and in primary mammospheres from different treatment groups.